



Elastoplastic torsion of hollow FGM circular shaft

Y. Bayat* and H. Ekhteraei Toussi

Faculty of Engineering, Ferdowsi University of Mashhad, Mashhad 9177948944-11, I. R. Iran

Article info:

Received: 03/10/2014

Accepted: 12/12/2014

Online: 03/03/2015

Keywords:

Functionally graded material,
Elastic-plastic analysis,
Torsion,
Hollow circular shaft,
Tamura-Tomota-Ozawa model.

Abstract

In many cases, a torsional shaft may be a thick-walled radially inhomogeneous cylindrical object. The hollow shafts made of functionally graded materials (FGMs) are such kind of compositions which were studied in this paper. Cylindrical FG shafts are composed of ceramic and metallic parts with power function distribution across the radial direction. The ceramic phase is isotropic elastic and the metallic phase was elastic-plastic. In this paper, the volume fraction-based elastic-plastic mixture rule of renowned Tamura-Tomota-Ozawa (TTO) was used to model the behavior of the composite material. The elasto-plastic torsion problem was modeled and solved analytically. The results were compared with the simulations of ABAQUS and the accuracy of the solutions was evaluated. Depending on the thickness and level of inhomogeneity, different modes of yielding were obtained. The results showed that plastic zone could occur at the inner or outer surfaces or simultaneously at both surfaces; even it may start in-between the thickness. Moreover, the influence of material inhomogeneity and thickness of shaft upon the plastic zone development were studied and discussed.

1. Introduction

The invention of new materials naturally creates new opportunities for the development of new kinds of structures. Controllable synthesis of two or more material parts for building heterogeneous compounds results in the development of new composite constructions, known as functionally graded materials (FGMs). These gadgets enable us to use more secure materials in the places, in which stresses are higher, or similarly use heat resistant compositions wherever the risk of burning, melting, or high conductivity is inevitable and probably keep the weight or price at its lowest level at the same time. On the other hand, in

line with the engineering and practical aspects of manufacturing processes, the analytical study of FGM structures attracts more attentions.

As in homogenous materials, the behavior of metallic-based FGMs includes both elastic and plastic characteristics. Comparing elastic analysis, down to high level of involved stresses and complex formulations so far the elastic-plastic analysis of FGMs has not attracted too much attentions. Thus, in this paper, the elastic-plastic study of FGM shafts was considered.

The first attempts for the elastic-plastic analysis of torsional shafts date back to the Saint-Venant's semi-inverse method used for the analyses of elastic torsion and very often for the

*Corresponding author

Email address: y.bayat.mech@gmail.com

study of elastic-plastic torsion of homogeneous shafts. Nadai [1] was the first who obtained the solution of elastic-plastic torsion of shafts. Based on a sand heap analogy, he obtained the stress field developed in a fully plastic shaft under torsional loads. By combining the membrane and sand heap analogies, Nadai [2] developed another approximate solution for the elastic-plastic torsion problems. Christopherson [3] presented a numerical solution for the elastic-plastic analysis of torsion in an I-sectioned shaft using finite difference method (FDM) and relaxation technique. Based on the stationary complementary energy principle and Rayleigh-Ritz expansion method, Smith and Sidebottom [4] presented an elastic-plastic analytical solution to the problem of torsion in rectangular shafts. Hodge [5, 6] studied the elastic-plastic torsion problem for the perfectly plastic materials using the non-linear programming technique. In another attempt, Hodge et al. [7] used non-linear programming in finite difference method (FDM) for the analysis of elastic-plastic torsion problems. The first attempts using finite element method (FEM) for the elastic-plastic analysis of torsional loading in uniform shafts date back to the works by Yamada et al. [8]. May and Al-Shaarbaf [9] developed FEM programs for the elastic-plastic analysis of uniform and non-uniform torsional members subjected to pure and warping torsions. In another attempt based on Mitre's method, the elastic-plastic solutions of torsion problem for various types of cross-sections were presented by Billingham et al. [10]. A number of imperative studies pertaining to the elastic and partially plastic torsion of prismatic tubes and bars have appeared in the publications of Wagner and Guttmann [11], Bakhshiani et al. [12], Sapountzakis and Tsipiras [13], and Kolodziej and Gorzelanczyk [14].

Despite various admirable elastic-plastic analyses of FGM structures such as the studies in [15–21], the elastic-plastic analytical investigations of yielding and deformation in hollow FGM shafts under torsional loads have not been considered thus far. Recently, Bayat et al. [22] studied the torsion of elastic hollow FGM cylinder. Material properties of the

cylinder were assumed to be the arbitrary functions of radial coordinate. They obtained the connection between shear stress and twist angle. Now, in order to extend the analyses of FGM shafts to the elastic-plastic region, the main objective of this paper was to propose an efficient method for the prediction of elastic, partially plastic, and fully plastic states of stress in a twisted FGM hollow shaft.

There may be two different approaches to propose the material properties of an FGM compound. One tactic is to find the overall mechanical properties according to the behavior of each constitutive part. Another approach does not tend to correlate material properties of the compound to those of its constituents. Instead, in this alternative approach, separate distribution functions are defined for each parameter and the analysis is done accordingly. For instance, in [15–19], radial distributions of the modulus of elasticity and yield strength are taken as power functions. Nemat-Alla et al. [20] proposed two-dimensional functionally graded compositions for the elastic-plastic analysis of 2D-FGM plate under thermal loading. In another work, Ozturk et al. [21] considered the parabolic variations of four material properties. These four properties including yield strength, modulus of elasticity, coefficient of thermal conduction, and thermal expansion coefficient are temperature insensitive, while Poisson's ratio is a constant unrelated to position or temperature. More recently, using the J_2 flow theory as the flow rule and TTO model of Tamura et al. [23] as the mixture rule of the ceramic/metal compounds, different elastic-plastic problems of stress analysis in FGM structures have been studied in [24–28].

This study was aimed to demonstrate the whereabouts of the plasticity start position and level of loading which leads to this condition. In this regard, different modes of plastic deformation were detected. The modes were controlled by the thickness and heterogeneity of the shaft. Different graphs were provided to illustrate these connections. According to the obtained results, there was a specific level of inhomogeneity (quantified by parameter n) which could control whether the starting point of plasticity depended on the shaft thickness or

not. Moreover, it was shown that whenever the initiation of plasticity was a thickness-depended phenomenon, the straining point of yielding would be located at the boundaries. Otherwise, when the heterogeneity level was higher than the critical value and insensitive to thickness, the commencing point of the plastic deformations definitely would be located inside the bulk of the material.

2. Governing equations

As shown in Fig. 1, consider a hollow thick wall shaft with the internal radius of 'a' and external radius of 'b' made of functionally graded material (FGM). All through the shaft, the axisymmetric distribution of material properties change continually in $a < r < b$.

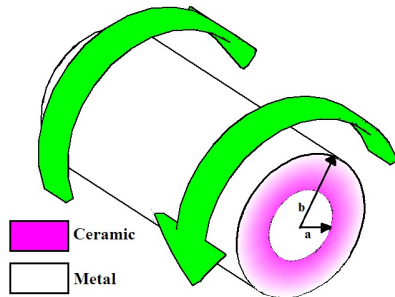


Fig. 1. A hollow FG circular shaft with internal radius a and external radius b .

As shown in Fig. 1, the two ends of a heterogeneous shaft are twisted with the relative amount of α radian per unit length in opposite directions. In order to describe the elastic-plastic behavior of the metal/ceramic FGM shaft, the intermediate law of mixture, originally proposed for the cemented carbides by Tamura *et al.* [23] (i.e. the TTO model), is utilized. Based on the TTO model, in a two-phase FGM structure, each material point is treated as a quasi-homogenous compound with the overall uniaxial stress σ and strain ε components related to the corresponding average uniaxial stress and the following strain of the constitutive parts:

$$\sigma = V_c \sigma_c + V_m \sigma_m, \quad \varepsilon = V_c \varepsilon_c + V_m \varepsilon_m \quad (1)$$

where σ_m and ε_m represent the average stress and strain of the metallic part, while σ_c and

ε_c are those of the ceramic part. Also, V_m and V_c are the volume fractions of the metal and ceramic constituents, respectively. A power function is used to introduce the radial distribution of volume fractions. In this case the volume fractions of the metal and ceramic phases is provided as:

$$V_m = \left(\frac{\bar{r} - 1}{k - 1} \right)^n; \quad V_c = 1 - V_m \quad (2)$$

In Eq. (2), 'n' is the inhomogeneity index, $\bar{r} = r/a$ is the relative position, and $k = b/a$ is a geometrical dimensionless parameter depending on the thickness of shaft. An additional parameter q is also used in the formulation of TTO model; i.e.:

$$q = \frac{\sigma_c - \sigma_m}{|\varepsilon_c - \varepsilon_m|}, \quad 0 \leq q \leq \infty \quad (3)$$

Parameter q is called "ratio of stress to strain transfer" [27] and its value depends on the mechanical properties and microstructural interactions of the constitutive parts. For example, q is zero if the constitutive elements have equal amounts of stress levels. When both parts experience an identical strain level in the loading direction, q will tend to $+\infty$. In general, because of the complex microstructural interactions and statistical scatter in the shape and orientation of the particles, the constitutive parts may neither undergo equal strains nor experience equal stress levels. In other words, a nonzero and finite value of q is generally more realistic than its extreme zero or infinite amounts. In practice, q may be approximately determined by numerical or experimental methods. For example, Bhattacharyya *et al.* [29] experimentally determined the typical value of 91.6 GPa for the q of Al/SiC compound.

In elastic deformation, both parts of the FG ceramic/metal compound behave elastically; i.e.:

$$\sigma_m = E_m \varepsilon_m, \quad \sigma_c = E_c \varepsilon_c \quad (4)$$

where E_m and E_c represent Young's moduli of the metal and ceramic constituents, respectively. Using Eqs. (1), (2), and (4), the overall Young's modulus, E , of the composite is obtained as:

$$E = \left[V_m E_m \frac{q + E_c}{q + E_m} + V_c E_c \right] / \left[V_m \frac{q + E_c}{q + E_m} + V_c \right] \quad (5)$$

In the TTO model, the overall Poisson's ratio, ν , follows a rule of mixtures; i.e.:

$$\nu = V_c \nu_c + V_m \nu_m \quad (6)$$

where ν_m and ν_c represent Poisson's ratio of the metal and ceramic constituents, respectively.

It is assumed that a power function can be used to model the uniaxial stress-strain behavior of the metallic phase beyond the yield point:

$$\varepsilon_m = \varepsilon_0 \left(\frac{\sigma_m}{\sigma_0} \right)^{n_0}, \quad \sigma_m \geq \sigma_0 \quad (7)$$

where $\varepsilon_0 = \sigma_0 / E_m$ and n_0 denote the yield strain and the hardening exponent of the metal, respectively. Schematics of power law metallic phase stress-strain curve and stress-strain line of perfectly elastic ceramic phase is shown in Fig. 2. In this figure, the intermediate curve located between the upper inclined line and lower bent curve is the result of the TTO homogenization.

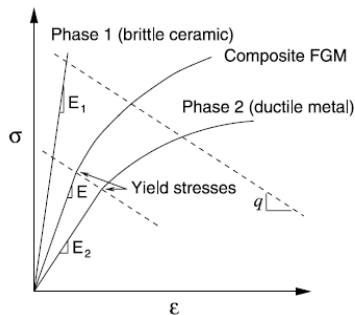


Fig. 2. Scheme of homogenization by the extended TTO model [23].

As in [27], the following parametric equations can be used to determine the stress-strain (σ - ε) curve of the mixture beyond the yield point:

$$\frac{\varepsilon}{\varepsilon_Y} = \frac{V_c E}{q + E_c} \frac{\sigma_m}{\sigma_Y} + \frac{(q + V_m E_c) E}{(q + E_c) E_m} \frac{\sigma_0}{\sigma_Y} \left(\frac{\sigma_m}{\sigma_0} \right)^{n_0} \quad (8a)$$

$$\frac{\sigma}{\sigma_Y} = \frac{V_m q + E_c}{q + E_c} \frac{\sigma_m}{\sigma_Y} + \frac{V_c q E_c}{(q + E_c) E_m} \frac{\sigma_0}{\sigma_Y} \left(\frac{\sigma_m}{\sigma_0} \right)^{n_0} \quad (8b)$$

where $\varepsilon_Y = \sigma_Y / E$ is the yield strain of the compound. Based on the TTO model, to determine the amount of yield stress for the compound, the resultant stress-strain curve

must be used. Accordingly, the yield stress σ_Y of the composite is determined as:

$$\sigma_Y(V_m) = \sigma_0 \left[V_m + \frac{q + E_m}{q + E_c} \frac{E_c}{E_m} V_c \right] \quad (9)$$

where σ_0 represents the yield stress of the metallic phase. Eq. (9) shows that the yield stress of the compound depends on the yield stress of the metal, volume fraction of constitutive parts, Young's modulus of each phase, and parameter q .

3. Elastic deformation and onset of yielding

In this section, after a review of the elastic deformations in FGM shafts, the conditions that control the whereabouts and twist levels required for the start of plasticity are studied. It will be observed how these simple requirements may lead to some unexpectedly ambiguous answers.

3.1. Elastic model and solution

For a circular hollow shaft, an axisymmetric-plane stress formulation leads to a one dimensional governing equation unrelated to angular coordinate θ . Similarly, in this axisymmetric analysis of FGM shafts, the warping function which is utilized in the analysis of non-circular shafts is not required [22, 30,31]. Under these conditions, the displacement components in the polar coordinate of (r - θ - z) can be represented as [22]:

$$u_r = 0 \quad (10a)$$

$$u_\theta = \alpha r z \quad (10b)$$

in which z axis coincides the axial direction of the shaft. Besides, u_r and u_θ are the displacement components in r and θ directions and α is the angle of twist per unit length. Eq. (10b) results in:

$$\gamma_{\theta z} = \alpha r \quad (11)$$

while all other strain components are zero. Here, the useful stress-strain relationship is:

$$\tau_{\theta z} = G \gamma_{\theta z} \quad (12)$$

where τ represents the only non-zero shear stress component and G is the shear modulus

which can be obtained by the well-known correlation of $G = E / 2(1 + \nu)$. By inserting Eq. (11) in (12), the shear stress component is formulated as:

$$\tau_{\theta z} = G\gamma_{\theta z} \tag{13}$$

Using this field of stress, the position of the yielding commencement radius across the radial direction can be obtained. This study is followed in the next section.

3. 2. Onset of plasticity

Torsional yielding of homogenous hollow circular shafts was studied by Mendelson [32]. The analyses showed that yielding always begins at the outer surface of a homogeneous shaft. But, in FGM hollow circular shafts, depending on the value of different materials and geometrical parameters, different modes of plastic flow may occur. In this case, plastic region may emerge at the inner surface, at the outer surface, in an intermediate radius between the inner and outer surfaces, and even at both inner and outer surfaces simultaneously. To locate the whereabouts of the yield initiation point, using the von Mises yield criterion, the yield criterion can be written in terms of the shear stress component as follows:

$$\tau_{\theta z} = \sqrt{3}\sigma_Y / 3 \tag{14}$$

By inserting $\tau_{\theta z}$ and σ_Y from Eqs. (13) and (9) in Eq. (14), the limit angle of twist per unit length in which yielding starts is obtained as:

$$\alpha_Y = \frac{2\sqrt{3}\sigma_Y(1+\nu)}{3Er} \tag{15}$$

Once the overall amounts of the parameters E , ν and σ_Y are replaced with their definitions provided in Eqs. (5), (6), and (9), consequently, Eq. (15) can be expanded as in the following form:

$$\alpha_Y = \frac{2\sigma_0(1+V_cV_c+V_mV_m)}{\sqrt{3}E_m r} \left[V_m + \frac{q+E_m}{q+E_c} V_c \right] \tag{16}$$

Seemingly, α_Y is the angle of twist per unit length which triggers the yielding at definite radius r . In other words, Eq. (16) demonstrates how much the shaft might be twisted before yielding can happen at radius r . But, whenever such a level of twist is applied to a shaft,

plasticity may have been already started at somewhere that needs a less amount of twist angle. It means that this definite value of $\alpha_Y = \alpha_Y(r)$ is not necessarily the specific value of twist angle which results in the yielding commencement. In other words, this angle of twist will show the yielding commencement twist angle only if its relevant radius ' r ' becomes the starting point of the plastic deformation. It is clear that, in a homogeneous shaft, this specific position is the largest radius for the cross-section; but, in heterogeneous shafts, its position must be obtained. All of these facts recommend that a specific procedure must be used to pinpoint the effective value of twist which can really start plastic deformations. To characterize that specific amount, the potential plastic twist level α_Y obtained in Equation (16) is primarily called yield twist. To obtain the effective yield twist level, the following procedure should be utilized.

Using Eq. (16) for a heterogeneous shaft, one can define a new parameter λ which can be used for the classification of yielding style. It is assumed that:

$$\frac{\alpha_Y|_{r=a}}{\alpha_Y|_{r=b}} = \frac{k}{\lambda} \tag{17}$$

where λ is a constant parameter as follows:

$$\lambda = \left(\frac{1+\nu_m}{1+\nu_c} \right) / \left(\frac{q+E_m}{q+E_c} \right) \tag{18}$$

In fact, for $k = \lambda$, Eq. (17) gives the specific condition $\alpha_Y|_{r=a} = \alpha_Y|_{r=b}$ which means that yielding emerges at the inner and outer surfaces simultaneously. In other words, considering Eq.(17) for $k < \lambda$, $k = \lambda$ and $k > \lambda$ results in $\alpha_Y|_{r=a} < \alpha_Y|_{r=b}$, $\alpha_Y|_{r=a} = \alpha_Y|_{r=b}$ and $\alpha_Y|_{r=a} > \alpha_Y|_{r=b}$, respectively. These inequalities mean that yielding starts from the inner surface for $k < \lambda$, whereas for $k > \lambda$, yielding starts at the outer surface. Also, for $k = \lambda$, yielding emerges at the inner and outer surfaces simultaneously. Indeed, this condition means that the radial position of yielding point can be affected by k . It means that k can be selected as a geometrical parameter to locate the yield start radius.

Based on Eq. (16) at the onset of yielding, there is a specific connection between the radial coordinate $r = r_Y$ and yield twist α_Y . At the same time, the previous discussions recommend that, for the specific radius $r = r_Y$, the curve of $\alpha_Y - r$ must experience a minimum. Obviously, that radius is the position, from which yielding can potentially perpetuate. That specific radius of yield commencement should be found. It can be realized that the value of parameter n , i.e. the inhomogeneity index in Eq. (2), is another factor which controls the starting position and torque of plastic deformation. In fact, for n bigger than a critical value, denoted by n_{cr} , plastic flow starts somewhere in the bulk of the shaft material, i.e. at radius $r = r_Y$ where $a < r_Y < b$. This critical value of n_{cr} plays an influential role in the classification of torsional problems and is obtained as follows.

As $\alpha_Y = \alpha_Y(r_Y, n_{cr})$, the critical value of n will be the minimum amount of n so that $\alpha_Y - r$ curve experiences a minimum at intermediate radius or $a < r_Y < b$. For the condition of minimum point in $\alpha_Y - r$ curve, the following can be written:

$$\text{at } r = r_Y \text{ and } n = n_{cr} : \frac{\partial \alpha_Y}{\partial r} = 0 \tag{19}$$

which results in,

$$\frac{\sigma'_Y(r_Y, n_{cr})}{\sigma_Y(r_Y, n_{cr})} - \frac{G'(r_Y, n_{cr})}{G(r_Y, n_{cr})} - \frac{1}{r_Y} = 0 \tag{20}$$

In Eq. (20), both n_{cr} and r_Y are unknown parameters. Therefore, another condition is required to determine n_{cr} and r_Y . But, if one plots the $\alpha_Y - r$ curves with different amounts of n as the parameter, at a specific amount of $n = n_{cr}$, the proper curve experiences a minimum at $a < r_Y < b$. To find the amount of $n = n_{cr}$, it is not difficult to imagine that the minimum angle of twist which causes yielding commencement at $a < r_Y < b$ is equal to the same twist angle which causes yielding onset at the inner or outer surfaces. This condition can be written as:

$$\alpha_Y(r_Y, n_{cr}) = \alpha_Y(a) \quad \text{for } k < \lambda \tag{21a}$$

$$\alpha_Y(r_Y, n_{cr}) = \alpha_Y(b) \quad \text{for } k > \lambda \tag{21b}$$

$$\alpha_Y(r_Y, n_{cr}) = \alpha_Y(a) = \alpha_Y(b) \quad \text{for } k = \lambda \tag{21c}$$

which results in:

$$\frac{\sigma_Y(r_Y, n_{cr})}{\sqrt{3}r_Y G(r_Y, n_{cr})} - \alpha_Y(a) = 0 \quad \text{for } k < \lambda \tag{22a}$$

$$\frac{\sigma_Y(r_Y, n_{cr})}{\sqrt{3}r_Y G(r_Y, n_{cr})} - \alpha_Y(b) = 0 \quad \text{for } k > \lambda \tag{22b}$$

$$\frac{\sigma_Y(r_Y, n_{cr})}{\sqrt{3}r_Y G(r_Y, n_{cr})} - \alpha_Y \Big|_{r=a \text{ or } r=b} = 0 \quad \text{for } k = \lambda \tag{22c}$$

Therefore, n_{cr} and r_Y can be determined by numerical solution of Eqs. (20) and (22). It should be noted that:

$$\text{at } r = r_Y \text{ and } n = n_{cr} : \frac{\partial^2 \alpha_Y}{\partial r^2} > 0 \tag{23}$$

Figure 3 and Table 1 summarize the process of finding the yielding onset radius for different FGM hollow circular shafts.

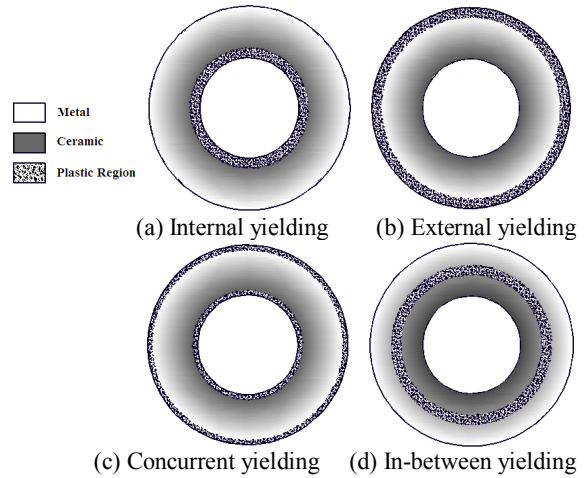


Fig. 3. Classifying yielding start position in FG hollow circular shafts.

Table 1. Comparing yielding onset radius in an FG hollow circular shaft under torsional loading.

	$0 < n < n_{cr}$		$n \geq n_{cr}$
	$k < \lambda$	$k = \lambda$	
$r_Y = b$	$r_Y = a$	$r_Y = a \text{ \& } r_Y = b$	$r_Y = b$
			$a < r_Y < b$

4. Ongoing elastic-plastic deformations

Once yielding is initiated, the linear elastic relation between the stress and strain components fades away. This inherent change of material in stress-strain correlation affects

the governing equations as well as the overall pattern of the stress distribution all over the body. In the axi-symmetric study of torsion problem, the pattern of deformation has been already provided in Eqs. (10). It shows that elastic-plastic study of the torsion problem only depends on the clear definition of the stress-strain relationship. Accordingly, this section is devoted to the introduction of material constitutive correlations, which leads to the analysis of progressive elastic-plastic deformation in the FGM shafts.

4. 1. Formulation

Assuming small stains, small deformations, and accumulative elastic-plastic strain hypothesis, the following can be written:

$$\gamma_{\theta z} = \gamma_{\theta z}^e + \gamma_{\theta z}^p \tag{24}$$

where $\gamma_{\theta z}^e$ and $\gamma_{\theta z}^p$ are the only nonzero elastic and plastic strain components, respectively. Using the deformation theory of plasticity and von Mises yield criterion, the equivalent plastic strain ε^p is obtained as follows:

$$\varepsilon^p = \gamma_{\theta z}^p / \sqrt{3} \tag{25}$$

Inserting Eqs. (11) and (12) in (24) and subsequently in (25) provides:

$$\varepsilon^p = (\alpha r - \frac{\tau_{\theta z}}{G}) / \sqrt{3} \tag{26}$$

Similarly, the equivalent von Mises stress is reduced to:

$$\sigma_e = \sqrt{3}\tau_{\theta z} \tag{27}$$

Now, using the provided stress-strain curve of $\sigma(\varepsilon)$, the equivalent von Mises stress produced by torsional loading or $\sigma_e(\tau_{r\theta})$ is reflected back onto the ordinate of the $\sigma(\varepsilon)$ curve; i.e.:

$$\sigma(\varepsilon) = \sigma_e(\tau_{r\theta}) \tag{28}$$

In this paper, $\sigma(\varepsilon)$ is obtained by the TTO model in Eq. (8b). Moreover, Eq. (27) is used for calculating $\sigma_e(\tau_{r\theta})$.

In the elastic-plastic analysis of structures, there is a similarity between the uniaxial stress-plastic strain curve and the equivalent stress-plastic strain curves. Therefore, before using the TTO model, the elastic strain components must be subtracted from the curve or equation to

obtain the $\sigma = f(\varepsilon^p)$ relationship. Considering Eq. (8a), the plastic part of the total strain in the TTO model can be obtained as:

$$\varepsilon^p = \varepsilon - \varepsilon^e \tag{29}$$

where ε is the total uniaxial strain in the TTO model of Eq. (8a) and ε^e denotes its total elastic part. The elastic portion of total strain is provided by:

$$\varepsilon^e = \sigma / E \tag{30}$$

In this study, the total strain is found by the deformation pattern in Eq. (10). Besides, there is a specific formula for the calculation of equivalent stress. Therefore, the amount of equivalent plastic strain can be found by inserting Eq. (27) in Eq. (28) and then in Eq. (26) to obtain:

$$\varepsilon^p = \frac{\alpha r}{\sqrt{3}} - \frac{\sigma}{3G} \tag{31}$$

Afterwards, inserting Eq. (30) in Eq. (29) and then equating the result with Eq. (31) provide:

$$\varepsilon = \frac{\alpha r}{\sqrt{3}} - \frac{\sigma}{3G} + \frac{\sigma}{E} \tag{32}$$

Here, it seems necessary to emphasize that the two terms $\sigma / (3G)$ and σ / E in Eq. (32) are not exactly equal. In fact, these two terms can be omitted if one assumes that elastic deformations are incompressible, which is not true.

Now, using the TTO model, inserting σ and ε from Eqs. (8a, b) in Eq. (32) results in:

$$\xi_1(r, n)\sigma_m + \xi_2(r, n)\left(\frac{\sigma_m}{\sigma_0}\right)^{n_0} = \frac{\alpha(q + E_c)}{\sqrt{3}}r \tag{33}$$

where

$$\xi_1(r, n) = \left(V_c + (V_m q + E_c) \left(\frac{1}{3G} - \frac{1}{E} \right) \right), \tag{34a}$$

$$\xi_2(r, n) = \left(q + V_m E_c + V_c q E_c \left(\frac{1}{3G} - \frac{1}{E} \right) \right) \frac{\sigma_0}{E_m}. \tag{34b}$$

Equation (33) can be numerically solved for the unknown parameter σ_m . Hence, the equivalent components of stress and strain can be obtained. Afterwards, using Eq. (31), the plastic strain ε^p is calculated. Finally, using the relationships between the equivalent and shearing components of strain and stress, the distribution of these fields is calculated.

4. 2. Method of elastic-plastic analysis

Analysis of non-homogenous structures in Section 3 indicates that, once the analysis of plasticity is the case, even the detection of starting radius of plasticity is a challenging task. In this case, depending on the inner and outer radii of shaft as well as the pattern of heterogeneity, different circumstances may happen. The following algorithm summarizes the procedure proposed for the identification of the initial yielding twist and the position of plastic deformation commencement radius.

• Step1.

For a given material and geometrical properties, given the angle of twist per unit length α , and using Eqs. (18), (20), and (22), λ and n_{cr} are determined.

• Step2.

If $n > n_{cr}$, plasticity starts somewhere in-between the thickness at radius $r = r_Y$. In this case, for a known n , r_Y is obtained by numerical solution of Eq. (20). Then, using Eq. (16), $\alpha_Y = \alpha_Y(r_Y)$ is obtained.

If $n < n_{cr}$, depending on the value of k , yielding may begin on the inner side or outer side or even simultaneously on both sides. Considering Eq. (17), in this case, $k < \lambda$ results in $\alpha_Y = \alpha_Y(a)$. Otherwise, if $k > \lambda$, yielding emerges on the outer side of the cylinder; i.e. $\alpha_Y = \alpha_Y(b)$. Finally, if $k = \lambda$, it can be seen that $\alpha_Y = \alpha_Y(a) = \alpha_Y(b)$. This condition indicates that plastic zone emerges from the interior and exterior sides simultaneously.

If $\alpha \leq \alpha_Y$, there is no plastic region and the distribution of shear stress can be obtained from Eq. (13).

For a given n , when $\alpha > \alpha_Y$, plastic region can be found using the next step.

• Step3.

When $\alpha > \alpha_Y$, if $n < n_{cr}$ and $k < \lambda$, by increasing α , plastic region expands from the inner surface. In other words, in this case, the cylinder will be composed of an internal plastic region located in $a \leq r \leq r_{ep}$ surrounded by an

elastic region in $r_{ep} \leq r \leq b$ with r_{ep} being the position of the elastic-plastic borderline. On the other hand, if $\alpha > \alpha_Y$ and $k > \lambda$, plastic region will spread from the outer surface. In this manner, elastic region is at $a \leq r \leq r_{ep}$ and plastic region is at $r_{ep} \leq r \leq b$. If $\alpha > \alpha_Y$ and $k = \lambda$, the cylinder is partially plastic; i.e. in this case, the cylinder is composed of an internal plastic region at $a \leq r \leq r_{epI}$, an elastic region between $r_{epI} \leq r \leq r_{epII}$, and another outer plastic region at $r_{epII} \leq r \leq b$, in which r_{epI} and r_{epII} are the positions of the elastic-plastic borderlines. When α increases, both inward and outward plastic regions are expanded toward the intermediate layers. r_{ep} can be obtained from the condition of $\tau_{\theta z}^e(r_{ep}) = \tau_{\theta z}^p(r_{ep})$. Here, the letters e and p stand for the elastic and plastic regions, respectively. By employing this condition and using Eqs. (13) and (27), r_{ep} can be obtained from the numerical solution of the following equation.

$$r_{ep} - \frac{\sigma_Y(r_{ep})}{\sqrt{3}\alpha G(r_{ep})} = 0 \quad a < r_{ep} < b \quad (35)$$

The elastic-plastic borderline is somewhere in which $\sigma_e = \sigma_Y$. For $k = \lambda$, there are two roots of Eq. (35) at $a < r_{ep} < b$.

If $n > n_{cr}$, the plastic zone must appear at intermediate radius ($r = r_Y$) between the inside and outside boundaries; by increasing the twist per unit length, it propagates in the opposite sides. In this case, the cylinder is composed of an interior elastic zone at $a \leq r \leq r_{epI}$, an intermediate plastic zone at $r_{epI} \leq r \leq r_{epII}$, and an exterior elastic region at $r_{epII} \leq r \leq b$. Here, the elastic-plastic borders r_{epI} and r_{epII} can be also obtained from Eq. (35).

For elastic region, using Eq. (13), the shear stress $\tau_{\theta z}$ can be easily calculated. However, for the plastic region, at first, Eq. (33) should be solved numerically to obtain σ_m . Then, using Eq. (31), for a specific angle of twist, the plastic

strain ε^p is calculated. Hence, the shear stress $\tau_{\theta z}$ is numerically obtained from Eq. (26).

5. Sample case study

Consider a hollow circular shaft under the action of a torsional torque. As in [17] the following dimensionless variables are used to reduce the number of variables and generalize the application of the results:

$$\bar{r} = \frac{r}{a}; \bar{\sigma}_y = \frac{\sigma_y}{\sigma_y(a)}; \bar{\tau} = \frac{\sqrt{3}\tau_{\theta z}}{\sigma_y(a)}; \bar{\alpha}_y = \frac{\alpha_y}{\alpha_y(a)}; \bar{\varepsilon}^p = \frac{E(a)\varepsilon}{\sigma_y(a)}. \tag{36}$$

In this study, the shaft material is an FGM cermet which changes gradually from a perfectly SiC ceramic phase inside the shaft to the perfectly metallic phase at the outside. The distribution of volume fraction imitates the power law pattern discussed in the previous sections. The SiC phase is an isotropic linear elastic material [28]. Elastic-plastic behavior of the homogenized Al/SiC material is found using the TTO formulation.

Table 2 [33] represents the material properties of the SiC and Al constitutive phases. Moreover, similar to Bhattacharyya *et al.* [29], a value of $q = 91.6\text{GPa}$ is used for the stress to strain transfer ratio to find the stress–strain (σ – ε) curves of Al/SiC layers. The only geometrical parameter needed in this analysis is the internal radius of the shaft which is $a = 40(\text{mm})$.

Table 2. Material properties of aluminum and silicon carbide constituents [33].

Materials	Young's modulus (GPa)	Poisson's Ratio	Yield stress (MPa)	Hardening exponent
Al	67	0.33	24	2
SiC	302	0.17	-	-

5. 1. Elasticity and onset of plasticity

To find the position of the starting point of plastic deformation in a purely elastic condition, using Eq. (16), the non-dimensional yield parameter λ is calculated as $\lambda = 2.821$. Hence, the critical twist per unit length is investigated for $k = 1.5 < \lambda$, $k = \lambda$,

and $k = 3.2 > \lambda$. Figs. 4 through 6 demonstrate the yield twist per unit length for $k = 1.5 < \lambda$, $k = \lambda$, and $k = 3.2 > \lambda$, respectively. The results are plotted for different values of heterogeneity exponent n . Yielding point for each n starts at the absolute minimum point of each relevant curve.

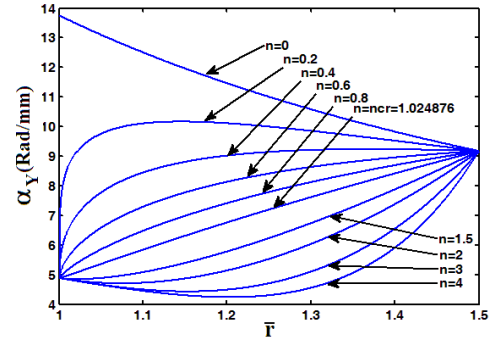


Fig. 4. Yield twist per unit length in radial direction ($k = 1.5 < \lambda$).

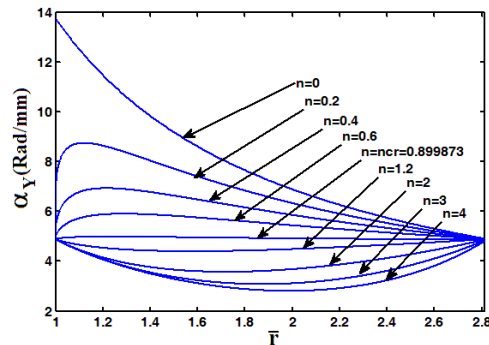


Fig. 5. Yield twist per unit length in radial direction ($k = \lambda$).

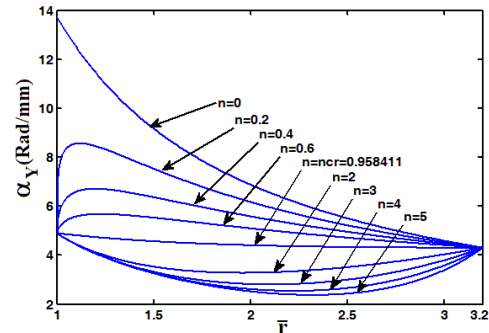


Fig. 6. Yield twist per unit length in radial direction ($k = 3.2 > \lambda$).

For example, considering Fig. 4, for $n=4$, the minimum twist which causes yielding in the cylinder is $\bar{\alpha}_y = 4.2312(\text{rad}/\text{mm})$ and starts at $r = r_y = 1.2026$. Therefore, for $n=4$, yielding emerges inside the cylinder. Indeed, according

to this figure for $n > n_{cr}$, plastic flow starts somewhere in-between the shaft cross-section, i.e. at $r = r_Y$, where $a < r_Y < b$ while for $n < n_{cr}$, yielding commences at the inner surface. Similarly, according to Figs. 5 and 6, for $n > n_{cr}$, plastic flow starts inside the cylinder; i.e. at $r = r_Y$, while for $n < n_{cr}$, yielding simultaneously commences at the inner and outer surfaces of Fig. 5 and at the outer surface of Fig. 6. Based on two exemplary pre- and post-critical amounts of heterogeneity exponent n , (i.e. $n = 0.8 < n_{cr}$ and $n = 4 > n_{cr}$), different graphs of yielding and shearing stresses are provided in the following section. It should be noted that, in each case, the dimensionless yielding and shearing stress functions are plotted for the minimum twist which causes the yielding.

5. 1. 1. Typical elastic analysis when $n < n_{cr}$

Figures 7-9 are plotted to demonstrate the radial distribution of dimensionless yield twist, yielding and shearing stresses for $n=0.8$.

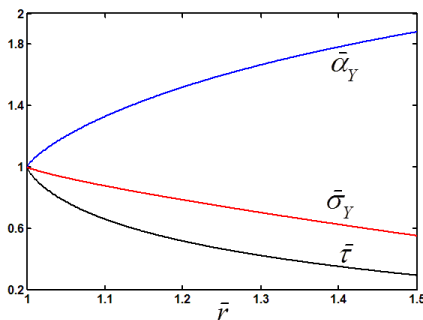


Fig. 7. Radial distributions of $\bar{\alpha}_Y, \bar{\sigma}_Y$, and $\bar{\tau}$ ($n = 0.8, k = 1.5$).

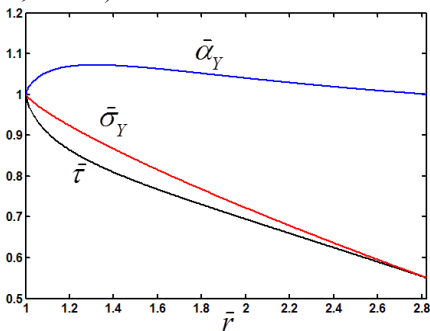


Fig. 8. Radial distributions of $\bar{\alpha}_Y, \bar{\sigma}_Y$, and $\bar{\tau}$ ($n = 0.8, k = 2.8$).

Considering the dimensionless parameters defined in Eq. (36), yielding occurs when $\bar{\tau} = \bar{\sigma}_Y$. According to Fig. 7, yielding starts at the inner surface for $k = 1.5$. Besides, this figure shows that yielding emerges from the point of minimum dimensionless twist at $\bar{\alpha}_Y = 1$. A similar pattern can be seen in Figs. 8 and 9. In Fig. 8, yielding starts at $\bar{\alpha}_Y = 1$, whereas in Fig. 9 yielding starts at $\bar{\alpha}_Y = 0.881592$, which is the lowermost point of the curve.

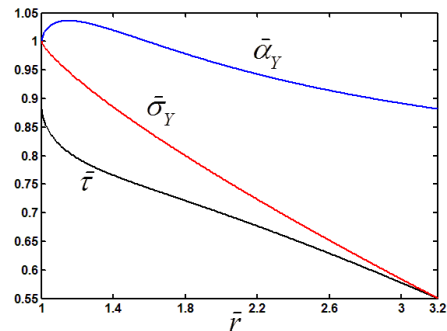


Fig. 9. Radial distributions of $\bar{\alpha}_Y, \bar{\sigma}_Y$ and $\bar{\tau}$ ($n = 0.8, k = 3.2$).

5. 1. 2. Typical elastic analysis when $n > n_{cr}$

Figure 10 shows the distribution of dimensionless yield twist, yielding, and shearing stresses in the radial direction for $n=4$. As is typical, since the behaviors of FG cylinder for $k < \lambda, k = \lambda$, and $k > \lambda$ for $n > n_{cr}$ are similar, the results are plotted for the sample $k = 1.5$.

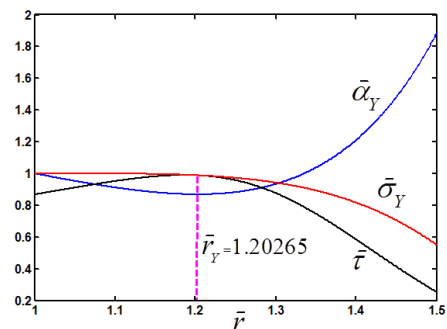


Fig. 10. Radial distributions of $\bar{\alpha}_Y, \bar{\sigma}_Y$ and $\bar{\tau}$ ($n = 4, k = 1.5$).

By obtaining the amount of minimum dimensionless twist in Fig. 10, the distributions

of dimensionless shear and yield stresses are plotted for $\bar{\alpha}_y = 0.86793$. Fig. 10 represents that yielding starts somewhere inside the cylinder. As is typical, here the start point is $\bar{r}_y = 1.20265$. It can be seen that the radius of yielding is the same point of minimum dimensionless twist.

5. 2. Developing plasticity

As discussed in Section 4, for a given material λ , depending on the geometrical parameter k , plastic region may emerge from inside, outside, concurrently from inside and outside, or somewhere in-between the cross-section. Hence, the dimensionless torsional shear stress in Figs. 7 through 10 are plotted for $\bar{\alpha}_y = 1, 1, 0.881592, 0.86793$, respectively. For $\bar{\alpha} > \bar{\alpha}_y$, the plastic region expands with increasing $\bar{\alpha}$. Therefore, similar to the preceding section, the results are prepared using $n = 0.8 < n_{cr}$ and $n = 4 > n_{cr}$.

5. 2. 1. Typical elastic-plastic analysis when $n < n_{cr}$

As shown in Fig. 7, assuming $n=0.8$ and $k=1.5$, the elastic yielding twist will be $\bar{\alpha}_y = 1$. Hence, for $\bar{\alpha} > \bar{\alpha}_y$, the plastic region expands from the inner surface with increasing $\bar{\alpha}$ and, at $\bar{\alpha}_{fp} = 1.88073$, the cylinder becomes fully plastic. Taking $\bar{\alpha}_y = 1.59712$, $\bar{r}_{ep} = 1.25$ can be found. Corresponding distribution of plastic strain as well as the dimensionless yielding and shearing stresses along the radial direction for $n = 0.8$ are plotted in Fig. 11. According to this figure, the cylinder is partially plastic composed of a plastic zone at $1 \leq \bar{r} \leq \bar{r}_{ep}$ and an elastic region at $\bar{r}_{ep} \leq \bar{r} \leq k$. Moreover, Fig. 11 shows that plastic strain is zero at the inner surface which complies with the elastic behavior of ceramic material in that position. For the cylinder with parameters $n=0.8$ and $k=2.81$ and twist value $\bar{\alpha} > 1$, yielding begins simultaneously at the inner and outer surfaces (see Fig. 8). Therefore, when $\bar{\alpha} > \bar{\alpha}_y$, by increasing $\bar{\alpha}$, plastic region expands from the

inner and outer boundaries and, at $\bar{\alpha}_{fp} = 1.072142662$, the cylinder becomes fully plastic at $\bar{r}_{fp} = 1.3147$. At $\bar{\alpha} = 1.0514$, the elastic-plastic interfaces are located at $\bar{r}_{ep1} = 1.8$ and $\bar{r}_{ep2} = 1.0843$. In this case, the relevant distributions of plastic strain, dimensionless yielding, and shearing stresses along the radial direction for $k=2.81$ are plotted in Fig. 12. According to this figure, the cylinder is partially plastic composed of plastic zone at $1 \leq \bar{r} \leq \bar{r}_{ep1}$ and $\bar{r}_{ep2} \leq \bar{r} \leq k$ and an elastic region at $\bar{r}_{ep1} \leq \bar{r} \leq \bar{r}_{ep2}$. Once again and because of the elastic behavior of the ceramic phase, it can be seen that plastic strain vanishes at the inner surface.

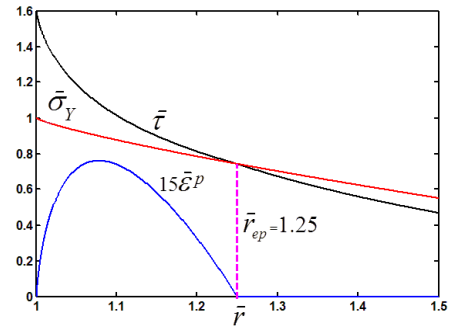


Fig. 11. Radial distributions of $\bar{\alpha}_y, \bar{\sigma}_Y$ and $\bar{\tau}$ ($n = 0.8, k = 1.5$).

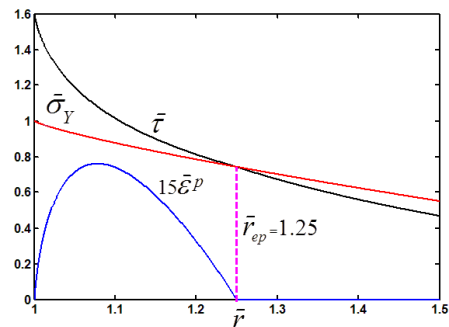


Fig. 12. Radial distributions of $\bar{\alpha}_y, \bar{\sigma}_Y$ and $\bar{\tau}$ ($n = 0.8, k = 2.8$).

For the cylinder with $n=0.8, k=3.2$, and $\bar{\alpha} > 0.881592$, yielding begins at the outer surface (see Fig. 8). At $\bar{\alpha}_{fp} = 1$, the cylinder becomes fully plastic. Assigning $\bar{\alpha} = 0.9593$, the elastic-plastic border is located at $\bar{r}_{ep} = 2$. The corresponding radial distributions of plastic

strain, dimensionless yielding, and shearing stress for $k=3.2$ are plotted in Fig. 13. According to this figure, the cylinder is partially plastic, composed of an elastic region at $1 \leq \bar{r} \leq \bar{r}_{ep}$ and a plastic zone at $\bar{r}_{ep} \leq \bar{r} \leq k$.

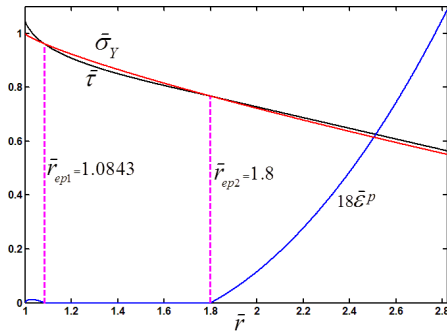


Fig. 13. Radial distributions of $\bar{\alpha}_Y$, $\bar{\sigma}_Y$ and $\bar{\tau}$ ($n = 0.8$, $k = 3.2$).

5. 2. 2. Typical elastic-plastic analysis when $n > n_{cr}$

Assuming $\bar{\alpha} = 1.59712 > \bar{\alpha}_Y$, Fig. 14 demonstrates the distribution of dimensionless plastic strain, yielding, and shearing stresses in the radial direction for $n=4$. As is typical, since the behavior of FG cylinder for $k < \lambda$, $k = \lambda$, and $k > \lambda$ for $n > n_{cr}$ are similar, the following results are plotted for $k=1.5$. It is seen that plastic strain emerges from $\bar{r}_Y = 1.20265$ and propagates towards the elastic-plastic borders at \bar{r}_{ep1} and \bar{r}_{ep2} .

5. 3. Validation

In this section, ABAQUS software is employed as a benchmark to compare the analytical results obtained from the present work using the FE method. Hereby, a hollow shaft was modeled using a commercial FE code, ABAQUS. Inner radius, outer radius, and length of the hollow shaft were 40, 60, and 5 mm, respectively. Similar to [22], an "8-node linear brick" element was used to represent the specimen. Down to longitudinal symmetry and without any conservation, the cylinder could be modeled as a short length cylinder (disk). First,

the homogenous case was considered. In this regard, setting $n=0$ in Eqs. (2) resulted in $V_m = 1$ and $V_c = 0$. It means that, for the homogeneous case, the shaft was made of purely aluminum metallic phase. The material properties provided in Table 2 were also used in the FE model. Moreover, the stress-strain (σ - ϵ) curve of the mixture beyond the yield point can be obtained from Eqs. (8). For applying the torsional load, one side of the cylinder was tied by a circular rigid plane and the torque was exerted in the center of circular rigid plane so that the angle of rigid plane rotation reached $\phi = 5.50120 \times 10^{-5}$ (Rad).

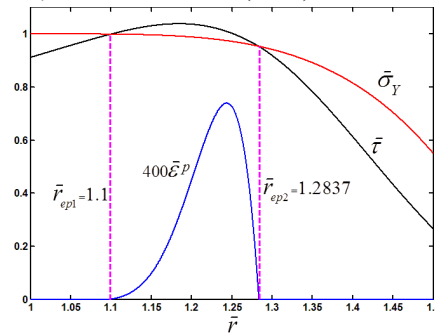


Fig. 14. Radial distributions of $\bar{\alpha}_Y$, $\bar{\sigma}_Y$ and $\bar{\tau}$ ($n = 4$, $k = 1.5$).

This amount of the rigid plane rotation yielded $\bar{\alpha}_Y = 0.8$. Besides, the circular plane was free to rotate about z-axis while constraining the other directions alone. Another side of the cylinder was fixed completely. Fig. 15 shows the meshing region.

Table 3 compares the dimensionless shear stress and plastic strain obtained by the FE method and the analytical solutions developed in this work for typical homogeneous ($n=0$) case. In Table 3, %Diff is defined as $\%Diff = \left| \frac{Anal. - FEM}{Anal.} \right| \times 100$. Based on Table 3, it

can be seen that the % Diff were relatively small and negligible almost in all cases. Moreover, according to Table 3, it is seen that, for the homogeneous hollow shaft, plastic strain emerged from outer surface and propagated towards the elastic-plastic border at $\bar{r}_{ep} = 1.25$.

In the second step, the FG thick walled shaft was modeled using ABQUS. In this regard, the

variation in material properties was implemented by dividing thickness into 20 layers with each layer having a constant value of the material properties [22, 34]. Here, the angle of rigid plane rotation $\phi = 3.89304 \times 10^{-5} (Rad)$ was considered. Assuming $n=0.8$, this amount of the rigid plane rotation yielded $\bar{\alpha}_y = 1.59712$. Table 4 shows a comparison between the analytical and FE results for dimensionless shear stress and plastic strain for typical $n=0.8$. It should be noted that the analytical FGM data for $n=0.8$ were extracted from Fig.11.

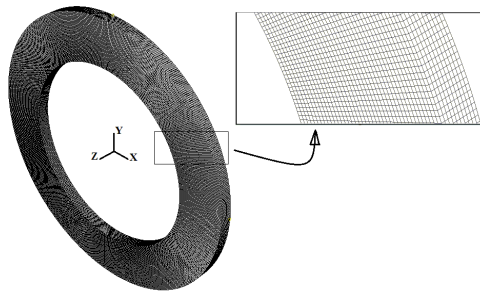


Fig. 15. Finite element mesh region.

According to Table 4, the % Diff were negligible almost in all cases, except for the inner and outer surfaces in which shear stress differences were increased up to 6.84%. The assumption of constant material properties in each layer led to such an error increase. Hereby, as the inhomogeneity index increased, the percentage of the error increased. Hence, the number of layers plays an important role in the accuracy of the FEM results.

Consequently, according to the assessments provided in Tables 3 and 4, it can be concluded the analytical method and solution were accurate and reliable.

6. Conclusions

An analytical technique was developed to find out what the twist level was and where the starting point of plastic deformation was in an FGM shaft under excessive rotations. The developed technique was used to analyze the elastic-plastic response of an FG circular

hollow shaft which obeyed the so-called homogenization rule of the Tamura–Tomota–Ozawa (TTO). The closed form solution was validated by the simulations of commercial ABAQUS software. The analytical results showed that, unlike the homogenous hollow circular shaft in which yielding initiates at the outer surface, in an FGM shaft depending on the level of geometrical parameter k and functionally graded parameter n_{cr} , different modes of yielding can be observed.

Table 3. Comparing the dimensionless shear stress and plastic strain obtained by the FE method and the analytical solutions developed in this work for $n=0$.

r/a	Type	$\bar{\tau}$		$\bar{\epsilon}^p$	
		Value	%Diff	Value	%Diff
1	Anal.	0.8000	0.625	0	----
	FEM	0.8050		0	
1.0875	Anal.	0.8700	0	0	----
	FEM	0.8700		0	
1.1875	Anal.	0.9500	0	0	----
	FEM	0.9500		0	
1.25	Anal.	1	0	0	----
	FEM	1		0.0532	
1.2875	Anal.	1.0140	0	0.6397	0.266
	FEM	1.0140		0.6414	
1.3875	Anal.	1.0503	0	2.3839	0.076
	FEM	1.0503		2.3857	
1.5	Anal.	1.0897	0.193	4.4072	2.552
	FEM	1.0876		4.2948	

Table 4. Comparing the dimensionless shear stress and plastic strain obtained by the FE method and the analytical solutions developed in this work for $n=0.8$.

r/a	Type	$\bar{\tau}$		$\bar{\epsilon}^p$	
		Value	%Diff	Value	%Diff
1	Anal.	1.5971	6.837	0	----
	FEM	1.4879		0.1445	
1.0875	Anal.	1.0510	0	0.5040	1.111
	FEM	1.0510		0.4984	
1.1875	Anal.	0.8315	0	0.2646	0.227
	FEM	0.8315		0.2652	
1.25	Anal.	0.7419	0.214	0	----
	FEM	0.7403		0.0422	
1.2875	Anal.	0.6890	0.526	0	----
	FEM	0.6854		0	
1.3875	Anal.	0.5719	0	0	----
	FEM	0.5719		0	
1.5	Anal.	0.4676	2.673	0	----
	FEM	0.4801		0	

It means that plastic zone may commence at the inner surface, at the outer surface, simultaneously at both surfaces, and even it may start somewhere in-between the thickness. In this work, proper analytical expressions were provided to characterize the decisive amounts of k and n_{cr} parameters. For different modes of incipient yielding, the elastic limit angle of twist was derived. Accordingly, it is possible to tailor the specific amounts of k and n to control the position of the elastic-plastic interface line. Moreover, stress analyses were extended to the plastic deformations. The partially plastic and fully plastic responses of the shaft were derived. The study showed that detection of the starting point of plastic deformations was a complex issue. On the contrary, because of the semi-inverse structure of the torsion problem, it was almost an easy task to analyze the stress field in the yielded region.

References

[1] A. Nadai, "Plasticity", *McGraw-Hill, New York*, (1931).

[2] A. Nadai, "Theory of Flow and Fracture of Solids", *McGraw-Hill, New York*, (1954).

[3] D. G. Christopherson, "A theoretical investigation of plastic torsion in an I-beam", *Journal of Applied Mechanics*, Vol. 7, No. 1, pp. 1-4, (1940).

[4] J. O. Smith and O. M. Sidebottom, "Inelastic behavior of load carrying members", *John Wiley & Sons, New York*, (1965).

[5] P. G. Hodge, "A deformation bounding theorem for flow-law plasticity", *Quarterly of Applied Mathematics*, Vol. 24, No. 1, pp. 171-174, (1966).

[6] P. G. Hodge, "Elastoplastic torsion as a problem in nonlinear programming", *international Journal of Solids Structure*, Vol. 3, No. 6, pp. 989-999, (1967).

[7] P. G. Hodge, C. T. Herakovich and R. B. Stout, "On numerical comparison in elastic- plastic torsion", *Journal of Applied Mechanics*, Vol. 35, No. 3, pp. 454-9, (1968).

[8] Y. Yamada, S. Katagiri and K. Katakryka, "Elastoplastic analysis of Saint-Venant torsion problem by a hybrid stress model", *International Journal for Numerical Methods in Engineering*, Vol. 18, No. 2, pp. 927-44, (1982).

[9] I. M. May and I. A. S. Al-Shaarbaf, "Elastoplastic analysis of torsion using a three- dimensional finite element model", *Computers & Structures*, Vol. 33, No. 3, pp. 667-78, (1989).

[10] A. Billinghamurst, J. R. L. Williams, G. Chen and N. S. Trahair, "Inelastic uniform torsion of steel members", *Computers & Structures*, Vol. 42, No. 6, pp. 887-94, (1992).

[11] W. Wagner and F. Gruttmann, "Finite element analysis of Saint-Venant torsion problem with exact integration of elastoplastic constitutive equations", *Computational Methods in Applied Mechanics and Engineering*, Vol. 190, No. 29-30, pp. 3831-48, (2001).

[12] A. Bakhshiani, M. Mofid, A. R. Khoei and S. L. McCabe, "Finite strain simulation of thin-walled tube under torsion using endochronic theory of plasticity", *Thin-Walled Structures*, Vol. 41, No. 5, pp. 435-59, (2003).

[13] E. J. Sapountzakis and V. J. Tsipiras, "Nonlinear inelastic uniform torsion of composite bars by BEM", *Computers & Structures*, Vol. 87, No. 3-4, pp. 151-66, (2009).

[14] J. AdamKolodziej and P. Gorzelanczyk, "Application of method of fundamental solutions for elastoplastic torsion of prismatic rods", *Engineering Analysis with Boundary Elements*, Vol. 36, No. 2, pp. 81-86, (2012).

[15] A. N. Eraslan and T. Akis, "Elastoplastic response of a long functionally graded tube subjected to internal pressure", *Turkish Journal of Engineering & Environmental Sciences*, Vol. 29, No. 6, pp. 361-368, (2005).

[16] T. Akis and A. N. Eraslan, "The stress response and onset of yield of rotating FGM hollow shafts", *Acta Mechanica*, Vo. 187, No. 1-4, pp. 169-187, (2006).

- [17] T. Akis, Elastoplastic analysis of functionally graded spherical pressure vessels, *Computational Materials Science*, Vol. 46, No. 6, pp. 545-554, (2009).
- [18] M. Sadeghian and H. EkhteraeiToussi, Axisymmetric yielding of functionally graded spherical vessel under thermo-mechanical loading, *Computational Materials Science*, Vol. 50, No. 3, pp. 975-81, (2011).
- [19] H. Ekhteraei Toussi and M. RezaeiFarimani, "Elastoplastic deformation analysis of rotating disc beyond its limit speed", *International Journal of Pressure Vessels and Piping*, Vol. 89, No. 1, pp. 170-77, (2012).
- [20] M. Nemat-Alla, K. Ahmed and Hassab-Allah I, "Elastic-plastic analysis of two-dimensional functionally graded materials under thermal loading", *International Journal of Solids and Structures*, Vol. 46, No. 14-15, pp. 2774-86, (2009).
- [21] A. Ozturk and M. Gulgec, "Elastic-plastic stress analysis in a long functionally graded solid cylinder with fixed ends subjected to uniform heat generation", *International Journal of Engineering Science*, Vol. 49, No. 10, pp. 1047-61, (2011).
- [22] Y. Bayat, M. Alizadeh and A. Bayat, "Generalized solution of functionally graded hollow cylinder under torsional load", *Journal of Computational and Applied Research in Mechanical Engineering*, Vol. 2, No. 2, pp. 23-33, (2013).
- [23] I. Tamura, Y. Tomota and H. Ozawa, "Strength and ductility of Fe-Ni-C alloys composed of austenite and martensite with various strength", In: *Proceedings of the Third International Conference on Strength of Metals and Alloys*, Cambridge: Institute of Metals, Vol. 1, No. 1, pp. 611-615, (1973).
- [24] A. T. Kalali and S. Hadidi, "A Semi-analytical Approach to Elastic-plastic Stress Analysis of FGM Pressure Vessels", *Journal of Solid Mechanics*, Vol. 5, No. 1, pp. 63-73, (2013).
- [25] R. L. Williamson, B. H. Rabin and J. T. Drake, "Finite element analysis of thermal residual stresses at graded ceramic-metal interfaces, Part I: model description and geometrical effects", *Journal of Applied Physics*, Vol. 74, No. 2, pp. 1310-20, (1993).
- [26] A. E. Giannakopoulos, S. Suresh, M. Finot and M. Olsson, "Elastoplastic analysis of thermal cycling: layered materials with compositional gradients", *Acta Metallurgica et Materialia*, Vol. 43, No. 4, pp. 1335-1354, (1995).
- [27] Z. H. Jin, G. H. Paulino and R. H. Dodds. "Cohesive fracture modeling of elastic-plastic crack growth in functionally graded materials", *Engineering Fracture Mechanics*, Vol. 70, No. 14, pp. 1885-1912, (2003).
- [28] R. Gunes, M. Aydin, M. K. Apalak and J. N. Reddy, "The elastoplastic impact analysis of functionally graded circular plates under low-velocities", *Composite Structures*, Vol. 93, No. 2, pp. 860-869, (2011).
- [29] M. Bhattacharyya, S. Kapuria and A. N. Kumar, "On the stress to strain transfer ratio and elastic deflection behavior for Al/SiC functionally graded material", *Mechanics of Advance Material Structure*, Vol. 14, No. 4, pp. 295-302, (2007).
- [30] C. O. Horgan and A. M. Chan, "Torsion of functionally graded isotropic linearly elastic bars", *Journal of Elasticity*, Vol. 52, No. 2, pp. 181-199, (1999).
- [31] H. Sadd, "Elasticity theory, applications, and numerics 2e", *Burlington, MA01803, USA*, (2009).
- [32] A. Mendelson, "Plasticity: Theory and Application", *The Macmillan Company, New York*, (1960).
- [33] M. Aydin, "An investigation on mechanical behaviors of functionally graded circular plates under low velocity impact loadings", *MSc Thesis, The Institute of Natural Sciences and*

Technology, Erciyes University, Kayseri,
(2009).

- [34] Y. Bayat, M. Ghannad and H. Torabi,
“Analytical and Numerical Analysis for

the FGM Thick walled sphere under
Combined Pressure and Temperature
Loading”, *Archive Applied Mechanic*,
Vol. 82, No. 2, pp. 229-242, (2012).